

Contents lists available at ScienceDirect

# Petroleum Science

journal homepage: www.keaipublishing.com/en/journals/petroleum-science



# Original Paper

# Evaluation of CO<sub>2</sub> storage in fractured coal seam and the effect of coal fines



Qian Wang <sup>a</sup>, Zhi-Jun Zhang <sup>b, \*</sup>, Jian-Long Xiong <sup>b</sup>, Jian Shen <sup>a</sup>, Paul W.J. Glover <sup>c</sup>, Piroska Lorinczi <sup>c</sup>

- <sup>a</sup> Key Laboratory of Coalbed Methane Resources and Reservoir Formation Process, Ministry of Education, China University of Mining and Technology, Xuzhou, 221008, Jiangsu, China
- <sup>b</sup> Sichuan Institute of Energetical and Geological Survey, Chengdu, 610072, Sichuan, China
- <sup>c</sup> School of Earth and Environment, University of Leeds, Leeds, LS2 9JT, UK

#### ARTICLE INFO

Article history:
Received 20 September 2024
Received in revised form
28 March 2025
Accepted 28 March 2025
Available online 29 March 2025

Edited by Yan-Hua Sun

Keywords:
Coal seam
Fractures
Coal fines
Blockage
CO<sub>2</sub> storage
Injection parameters

#### ABSTRACT

Gas channeling in fractures during CO2 injection into the deep coal seam seriously reduces the CO2 storage efficiency after the development of coalbed methane. The generation and migration of coal fines causes blockages in the fractures in the stage of drainage and gas production, reducing the gas channeling effect of injected CO<sub>2</sub> caused by the heterogeneity of the coal seam. To explore the impact of coal fines within coal seam fractures on the efficacy of CO2 storage, experiments on the production stage and CO<sub>2</sub> injection for storage were conducted on coal combinations containing propped fractures, fractures, and matrix. The CO<sub>2</sub> storage characteristics of coal at the constraint of coal fines, as well as the influence of multiple rounds of intermittent CO<sub>2</sub> injection and different injection parameters on the CO<sub>2</sub> storage effect, were analyzed. The research results show that blockage by coal fines increases the resistance to fluid flow in the fractures by 71.2%. The CO<sub>2</sub> storage capacity and storage potential of coal with coal fines are 6.5 cm<sup>3</sup>/g and 8.8% higher than those of coal without coal fines, while the CO<sub>2</sub> storage capacity of fractured coal under the influence of coal fines has the largest increase of 9.4 cm<sup>3</sup>/g. The CO<sub>2</sub> storage of coal containing coal fines is significantly higher (6.6%) than that of the coal without coal fines. The CO<sub>2</sub> storage effect of the coal with coal fines is improved with the increase in injection rate, whereas the CO<sub>2</sub> storage effect of the coal without coal fines decreases significantly (by 7.8%). Multiple rounds of intermittent injection increases the CO<sub>2</sub> storage volume of coal by 20.4% (with coal fines) and 17.1% (without coal fines). The presence of coal fines in fractures also slows down the downward trend of CO<sub>2</sub> storage fraction after multiple rounds of CO2 injection. The blockage in fractures significantly increases the CO2 injection time and difficulty, but can increase the CO<sub>2</sub> storage fraction by 4.7%-17.1%, and the storage volume by 1.9%-14%, increasing the feasibility of CO<sub>2</sub> storage in fractured coal seams that have previously been exploited for methane production. The multiple rounds of intermittent CO2 injection and shut-in periods has shown potential for greater CO<sub>2</sub> storage and injection efficiency.

© 2025 The Authors. Publishing services by Elsevier B.V. on behalf of KeAi Communications Co. Ltd. This is an open access article under the CC BY-NC-ND license (http://creativecommons.org/licenses/by-nc-nd/4.0/).

### 1. Introduction

Deep coal seams are widely distributed in China, and they represent a great potential for both the development of coalbed methane resources and  $CO_2$  storage (Li et al., 2018; Qin et al., 2020). Partially produced methane production wells can be converted to inject  $CO_2$  in the late stage of coalbed methane development, which

permeability can be as low as 0.0001 mD or even lower in deep coal seams with high stress or underdeveloped fractures, categorizing them as ultra-low porosity and ultra-low permeability reservoirs (Li et al., 2023; Lin et al., 2024). Hydraulic fracturing and other measures are commonly used to enable the economical and

not only improves the overall recovery of CH<sub>4</sub> from the coal seam, but also achieves significant CO<sub>2</sub> storage (Fan et al., 2019a, 2019b,

2021; Zhang and Ranjith, 2019). Deep coal reservoirs exhibit poor

reservoir properties, typically with matrix porosity ranging from

2.0% to 6.5% and permeability ranging from 0.001 to 0.1 mD. The

E-mail address: cugzhijun@163.com (Z.-J. Zhang).

<sup>\*</sup> Corresponding author.

Q. Wang, Z.-J. Zhang, J.-L. Xiong et al. Petroleum Science 22 (2025) 2502-2515

efficient extraction of coalbed methane (Clarkson and Bustin, 2010: Ma et al., 2022). One of the unfortunate results of inducing fracture systems is that the high-permeability channels that are formed lead to an increase in heterogeneity of fluid flow within the coal seam. The heterogeneity induced by the fracturing may potentially result in injected CO<sub>2</sub> flowing directly from injection wells to production wells along high-flow rate fracture channels (Song et al., 2018: Zhang et al., 2021), leading to limited access of the injected  $CO_2$  to the coal matrix, where it can be adsorbed and stored, as well as early break-through at production wells. This is a very inefficient way of attempting to store CO<sub>2</sub>. Consequently, gas flow heterogeneity in fractured coal seams is a key factor in determining the feasibility of CO<sub>2</sub> injection and storage. Intuitively, it would be optimal for injection and production wells to straddle the dominant fracture direction, rather than having the fractures directly linking the injection and production wells.

Coal fines are produced to varying degrees in coal seams during drilling, fracturing, and coalbed methane drainage stages. They have a wide particle size distribution, ranging from tens of nanometers to several millimeters (Cheng and Pan, 2020; Wang et al., 2023), and are carried by the fluid and transported, causing blockage in the natural and induced fracture systems (Wang Z. et al., 2021). The migration of coal fines is a typical issue in coalbed methane development research. The mechanism of coal fines transport and blockage is characterized using mathematical models simulation displacement experiments gas-liquid-solid three-phase flow model, visualization simulation of coal fines migration using a visualization model, experiments on coal fines migration in fractured core samples (Han et al., 2024; Guo et al., 2016). It was found that gas-water two-phase flow has a strong disturbance effect on coal fines, causing them to be activated and carried by the fluid. The water phase is highly effective at transporting coal fines. The transported coal fines can easily redeposit in the narrow parts of fractures, leading to blockages that significantly reduce the fracture conductivity (Huang et al., 2024; Zhu et al., 2017).

The blockage of coal fines can significantly affect coalbed methane production as well as CO<sub>2</sub> storage through several competing mechanisms (Guo et al., 2018). Coal fines can block fractures completely or partially, leading to reductions in both methane production and CO<sub>2</sub> injection. However, the inhibition of gas flow by coal fines can increase the volume of CO<sub>2</sub> that can be injected and stored because the injected CO<sub>2</sub> flows into the matrix more, interacting with the coal surfaces there, and being adsorbed (Cheng et al., 2021; De Silva et al., 2012). Consequently, it is important to study the influence and mechanism of coal fines retention in fractures on the CO<sub>2</sub> storage characteristics of the coal seam during CO<sub>2</sub> injection, in order to lay the foundation for demonstrating the feasibility of CO<sub>2</sub> storage by CO<sub>2</sub> injection into fractured coal seams in the late development stage.

The adsorption of CO<sub>2</sub> onto coal surfaces takes time. The rate of CO<sub>2</sub> adsorption onto coal depends on pressure, temperature, and the size of the coal surface area. The geometric shape of coal is a determining factor for the rate of CO<sub>2</sub> adsorption under the same conditions. Experimental results show that the rate of CO<sub>2</sub> adsorption by coal fines is more than 50 times that of coal in small blocks (Busch et al., 2004; Feng et al., 2021; Sun et al., 2021). Additionally, diffusion time of CO<sub>2</sub> from fractures into the matrix also has an effect. As a consequence, coal seams cannot adsorb CO<sub>2</sub> until fully saturated during the short CO<sub>2</sub> injection periods (Du et al., 2021; Wang et al., 2020; Yang et al., 2022). As a result, the full CO<sub>2</sub> storage potential of the coal seam is not fully utilized.

A multi-cycle intermittent gas injection technique has been proposed to address this problem, allowing more time for coal to adsorb CO<sub>2</sub>, while also reducing ineffective CO<sub>2</sub> circulation caused

by gas flowing predominantly through the fractures (Jin et al., 2021; Rezk and Foroozesh, 2022; Rezk et al., 2023). Consequently, exploring the influence of injection parameters and intermittent CO<sub>2</sub> injection on the CO<sub>2</sub> storage effect in coal seams considering the constraint of coal fines retention in the fractures is essential for efficient CO<sub>2</sub> injection and storage in fractured coal seams.

In this paper, anthracite samples from the Oinshui Basin, China. were prepared to represent coal with propped fractures, unpropped fractures, and the unfractured coal matrix. The coalbed methane drainage, gas production, and CO<sub>2</sub> storage experiments were carried out on the coal sample combinations both with and without coal fines occupying the fractures. Variations in flow resistance caused by coal fines blockage in the fractures were observed, and the CO<sub>2</sub> storage ability of propped fractures, unpropped fractures, and coal matrix samples, both with and without coal fines, were compared. The influence of coal fines on the ability of coal seams to store CO<sub>2</sub> at different injection pressures, injection speeds, and in multiple intermittent CO<sub>2</sub> injection processes was also studied. Theoretical and experimental data support was provided for evaluating the feasibility and storability of injected CO<sub>2</sub> after the coal seam is fractured for coalbed methane development was also considered.

# 2. Methodology

#### 2.1. Materials

The research target reservoir is the #3 coal seam in the southern part of the Qinshui Basin (south-eastern Shanxi Province, China), which occurs at a depth of 800-1300 m and temperatures between 41.6 and  $53.8\,^{\circ}$ C. It is very difficult to obtain large coal samples from such depths. Consequently, the anthracite samples used in our experiments were all collected from a large coal block sample at a depth of 712 m in the #3 coal seam of the Lu'an Yuwu Coal Mine. Its properties are shown in Table 1, where  $R_{0,\text{max}}$  is the maximum vitrinite reflectance value when using polarized light and is a measure of coal maturity; and  $M_{\text{ad}}$ ,  $A_{\text{ad}}$ ,  $V_{\text{daf}}$ ,  $FC_{\text{ad}}$  are fractions of moisture (water), ash, volatiles, and fixed carbon in the coal, respectively, summing to  $100\,\text{wt}\%$  (Zhang et al., 2023).

The large coal block sample was cut using a wire-cutting method to obtain seven cylindrical coal samples with uniform size and similar physical properties. These samples were prepared to facilitate comparative experiments exploring the CO<sub>2</sub> storage characteristics of coal, focusing on the CO<sub>2</sub> storage characteristics of coal with and without coal fines in fractures. The basic parameters for each sample are shown in Table 2. Among these, coal samples P1, P2, F1, F2, M1, and M2 were used for CO<sub>2</sub> storage experiments, and coal sample AQ was used in maximum CO<sub>2</sub> adsorption capacity tests.

The brine used in the experiment was prepared in the laboratory according to the formation water data, the main cations were  $\text{Ca}^{2+}$ ,  $\text{Na}^+$ ,  $\text{K}^+$ , and  $\text{Mg}^{2+}$ ; the main anions were  $\text{Cl}^-$ , and  $\text{HCO}_3^-$ . The formation water salinity was 5000 mg/L, and the water type was calcium chloride type.

### 2.2. Coal sample preparation

In experimental core flooding, the scale of the core is smaller, these processes of fluid flow take less time to develop to their fullest extent than they would at the field scale. Consequently, the drainage and gas production stage for the core flooding is shorter than that in the actual coal seam, and the amount of coal fines produced from the coal sample is much less.

In this work some of the coal samples had their fractures preloaded with coal fines before the experimental simulation of the

**Table 1** Analysis of coal composition.

| Coal rank  | Source        | R <sub>o,max</sub> , % | $M_{\rm ad}$ , wt% | $A_{\rm ad}$ , wt% | $V_{ m daf}$ , wt% | FC <sub>ad</sub> , wt% |
|------------|---------------|------------------------|--------------------|--------------------|--------------------|------------------------|
| Anthracite | Qinshui Basin | 2.83                   | 0.38               | 8.12               | 9.58               | 81.92                  |

**Table 2**Basic parameters of the coal cores.

| Coal number | Length, cm | Diameter, cm | Mass, g | Porosity, % | Permeability, 10 <sup>-3</sup> μm <sup>2</sup> | Type of coal sample prepared                       |
|-------------|------------|--------------|---------|-------------|--|--|
| P1          | 9.64       | 5.041        | 275.3   | 4.58        | 0.084  | Propped fracture with coal fines                   |
| P2          | 9.57       | 5.027        | 278.4   | 4.46        | 0.082  | Propped fracture without coal fines                |
| F1          | 9.62       | 5.031        | 276.6   | 4.64        | 0.086  | Unpropped fracture with coal fines                 |
| F2          | 9.57       | 5.028        | 274.7   | 4.65        | 0.088  | Unpropped fracture without coal fines              |
| M1          | 9.58       | 5.021        | 286.5   | 4.77        | 0.087  | Matrix coal  |
| M2          | 9.53       | 5.015        | 288.6   | 4.89        | 0.086  | Matrix coal  |
| AQ          | 9.59       | 5.026        | 283.3   | 4.56        | 0.083  | Coal for CO <sub>2</sub> adsorption capacity tests |

drainage and gas production stage. The state of coal fines migration and blockage in the fractures at the end of water drainage and gas production can better simulate the distribution of coal fines retained in the fractures before the CO<sub>2</sub> injection into the actual coal seam. Other fractured coal samples were measured without preloading coal fines in order to act as control samples, so that the influence of coal fines in the fractures on CO<sub>2</sub> storage could be measured. Different types of coal samples were prepared using a wire-cutting method. Among these, coal samples P1, P2, F1, and F2 were cut axially into two equal parts. The cutting process was intended to simulate a fracture. The preparation process of propped and unpropped fractured cores is shown in Fig. 1.

A mixture of quartz sand and coal fine particles was prepared to be placed in the 'fractures' between the two halves of certain samples. The quartz sand was consistent with the 40-80 mesh quartz sand proppant used during on-site fracturing operations. Synthetic coal fines were prepared by grinding and sieving anthracite samples to obtain a mesh size of 100-350 mesh, according to the particle size characteristics of the coal fines (150-350 mesh) produced in the coal seam (Shi et al., 2018). Because smaller coal fines are more easily transported and produced, it is possible that relatively larger coal fines may become trapped in the fractures. Therefore, the size range of coal fines placed in fractures during the experiment was appropriately expanded during the process. The mass fraction ratio of quartz sand to synthetic coal fines in the mixture during the experiment was set to 4:1, which was chosen with reference to the measured mass ratio of proppant to coal fines output from the coal seam (Wei et al., 2019; Zhu et al., 2023). Only quartz sand without coal fines was used as the fracture filling material in some samples. It is worth noting that the effect of CO<sub>2</sub> adsorption by coal fines on the experimental results was neglected, considering that the mass of coal fines in the fractures is much smaller than the mass of the coal

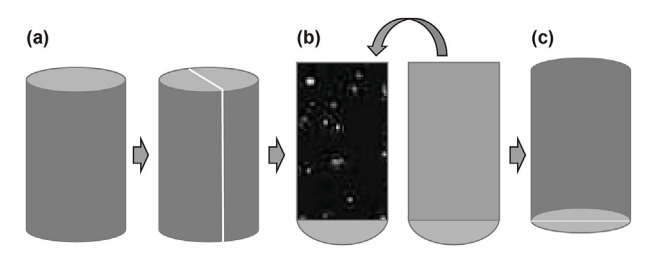


**Fig. 1.** The preparation process of propped fracture and unpropped fracture cores. (a) Core wire sawing, (b) the placement of coal fines and proppant, (c) the fixation of core with heat shrink films.

core combination and the volume of  $CO_2$  adsorbed by coal fines was much lower than that adsorbed of coal pillars.

In each case, the filling, if present, was added to one surface of the fracture to the desired thickness before placing the other half of the sample on it (Hu et al., 2020; Yang et al., 2018). For sample P1, the filling was a mixture of quartz sand and coal fines with a thickness of 3 mm. This sample represents a hydraulically fractured coal that produces coal fines. For sample P2, the filling consisted only of quartz sand, with no coal fines, with a thickness of 3 mm. This sample represents a hydraulically fractured coal producing no coal fines. For sample F1, the filling consisted only of coal fines with a thickness of about 0.5 mm, representing a naturally fractured sample containing coal fines. The final fractured sample, F2, which was given no filling, represents a naturally fractured sample that produces no coal fines.

Finally, each of the samples was wrapped in heat-shrink film. The heat-shrinkable film was heated to secure the coal sample. In addition, unfractured coal samples, M1 and M2, were prepared to examine the experimental results from a homogeneous, unfractured matrix (matrix coal sample). A seventh sample, AQ, was also prepared and used for adsorption tests.

# 2.3. Method for evaluating CO<sub>2</sub> storage capacity in coal

The ability of coal to store  $CO_2$  when injected with  $CO_2$  was evaluated using the following parameters: (i)  $CO_2$  storage capacity,  $S_p$ , which is defined as the volume of  $CO_2$  per unit mass of coal, (ii)  $CO_2$  storage fraction, F, which represents the percentage of the injected gas that is stored, and (iii) the extent to which the maximum  $CO_2$  storage potential of coal is exploited during the injection period, which is referred to as the fractional  $CO_2$  storage potential.

To compare the capacity of CO<sub>2</sub> stored in different coal samples, the CO<sub>2</sub> storage capacity,  $S_p$ , is defined as the volume of CO<sub>2</sub> stored per unit mass of coal (at standard conditions, 25 °C and 0.1 MPa),

$$S_{\rm p} = \frac{V_{\rm s}}{m} \tag{1}$$

where  $S_p$  represents the  $CO_2$  storage capacity,  $cm^3/g$ ;  $V_s$  is the volume of  $CO_2$  stored in coal during the test,  $cm^3$ ; and m is the mass of coal used in the test, g.

The CO<sub>2</sub> storage fraction, *F*, refers to the percentage of the volume of CO<sub>2</sub> stored in coal to the total volume of injected CO<sub>2</sub>, which is used to characterize the utilization efficiency of CO<sub>2</sub> during the injection process,

$$F = \frac{V_{\rm S}}{V_{\rm i}} \times 100\% \tag{2}$$

where F is the  $CO_2$  storage fraction, %;  $V_i$  is the injected  $CO_2$  volume,  $cm^3$ .

Due to the short injection process of CO<sub>2</sub>, the volume of CO<sub>2</sub> stored in coal failed to reach its maximum CO<sub>2</sub> storage capacity (Zhang and Ranjith, 2019). The extent to which the CO<sub>2</sub> storage capacity of coal is exploited during the injection period is characterized by the fractional CO<sub>2</sub> storage potential

$$P_{\rm d} = \frac{S_{\rm p}}{S_{\rm pm}} \times 100\% \tag{3}$$

where  $P_d$  is the fractional CO<sub>2</sub> storage potential, %;  $S_{pm}$  is the maximum CO<sub>2</sub> storage capacity of coal, cm<sup>3</sup>/g.

The maximum CO<sub>2</sub> storage capacity of coal, S<sub>pm</sub>, can be obtained through experiments (Lin et al., 2023; Xiong et al., 2024). The free space volume in the core holder was measured using an iron core before the tests. Coal sample AQ was placed in a core holder, and CO<sub>2</sub> was continuously injected into it under a confining pressure of 15 MPa and 50 °C to test the maximum CO<sub>2</sub> adsorption capacity of the coal sample under different equilibrium pressures. The purpose of the tests was to simulate the ability of block coal to store CO2 under reservoir conditions, rather than the conventional tests of CO<sub>2</sub> adsorption by coal particles. The results are shown in Fig. 2. Since CO<sub>2</sub> injection pressure in this work was 12 MPa and the constant back pressure was 10 MPa, it is expected that the maximum CO<sub>2</sub> storage capacity of the coal samples will be  $60\pm2$  cm<sup>3</sup>/g of rock at these pressures and 50 °C. The test duration was approximately 90–180 h. Although it involved testing the CO<sub>2</sub> adsorption process of coal blocks under stress conditions, the adsorption process is relatively short due to the continuous replenishment of CO<sub>2</sub> into the coal.

# 2.4. Experimental apparatus and procedure

The experimental apparatus is composed predominantly of a displacement system, a fluid collection and metering system, a data

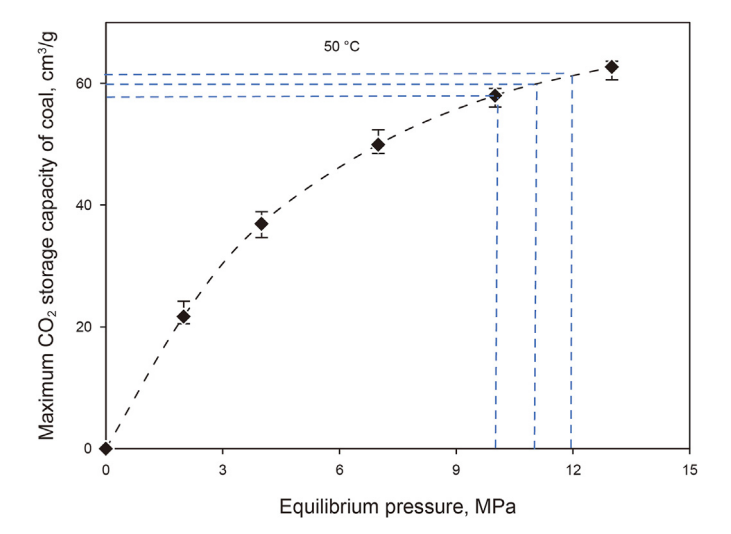


**Fig. 2.** Maximum  $CO_2$  storage capacity of coal samples at different equilibrium pressures and 50 °C. The dashed black line represents the trend of the data points. The fluid pressures experienced by the rock samples vary between 10 MPa (the back pressure at the output face) and 12 MPa (the injection pressure). These values give rise to maximum storage capacities of  $60\pm2$  cm<sup>3</sup>/g.

acquisition system, and a temperature control system. A schematic diagram of the experimental apparatus is shown in Fig. 3.

The CO<sub>2</sub> injection experiment consists of 7 steps.

- (1) The transfer tanks were filled with brine, CO<sub>2</sub>, and CH<sub>4</sub>, and the core holders were placed in a thermostat, with the temperature set to 50 °C for 24 h before the experiments.
- (2) Experiments were carried out using three samples at a time in order to mimic the situation in the reservoir as closely as possible. Each group of 3 samples was a sample combination. The prepared coal samples P1, F1, and M1 were placed into three core holders, left to right, respectively, to form a coal sample combination containing coal fines, where the first sample encountered by the injected gas is the propped fracture (in Core holder 1) followed by the unpropped fracture (in Core holder 2), and finally the unfractured matrix (Core holder 3). The cores were vacuumed and then saturated with CH<sub>4</sub> at a pressure of 0.5 MPa (the bottom hole flowing pressure) and the confining pressure of 1 MPa before the experiment.
- (3) The confining pressure was set to 15 MPa. The switch connected to the gas—liquid separator on the right side of each holder was closed at this point, and brine was injected into the coal sample combination from the right end of Core holder 3 at a rate of 2 mL/min for 5 h with the back pressure of 0.5 MPa. The brine was produced from the left end of Core holder 1 to simulate the drainage stage and the process of coal fines migration to production wells in coal seams.
- (4) Humidified CH<sub>4</sub> was injected in the same direction at a speed of 2 mL/min (at  $P_{\rm conf} = 15$  MPa and T = 50 °C) to displace the water in the coal sample combination. The total CH<sub>4</sub> injection time was 5 h to simulate the CH<sub>4</sub> production stage in conventional coal seam gas extraction.
- (5) The back pressure was then set to 10 MPa, and CO<sub>2</sub> was injected continuously from the left end of Core holder 1 with an injection pressure difference of 2 MPa, collecting the produced gases from the right-hand end of Core holder 3, and performing chromatographic detection until the produced gas was completely CO<sub>2</sub>. The total injection time was 13.1 h.
- (6) The valves were closed at both ends of each of the three core holders, and the pressure decay process in the holders was recorded. After the pressure decay stage, the CO<sub>2</sub> stored in each of the coal samples was recorded. The values of S<sub>p</sub>, F, P<sub>d</sub> were primarily calculated based on data such as the injected CO<sub>2</sub> volume, the produced CO<sub>2</sub> volume, the volume of CO<sub>2</sub> desorbed and released from the coal after the experiment, and the adsorption test results of the AQ samples (Fig. 2).
- (7) After the experiment, the propped fracture and unpropped fracture of the coal sample were divided into four equal portions along the CO<sub>2</sub> injection direction in order to (i) collect the coal fines, (ii) rinse and separate the quartz sand, (iii) collect the flushing liquid to prepare a coal fines solution to test its concentration using the ultraviolet—visible spectrophotometry method, and (iv) observe the change in the fracture morphology. The coal fines distribution was, hence, measured as a function of sample type, location within each sample type and fracture.

Steps (1) to (6) were repeated to conduct experiments on the P2-F2-M2 coal sample combination, which does not contain coal fines. The injection pressure and final injected  $CO_2$  volume were the same as the P1-F1-M1 combination. In addition, steps (1) to (5) were repeated to carry out  $CO_2$  injection and storage experiments at an injection pressure of 8–13 MPa and an injection flow rate of

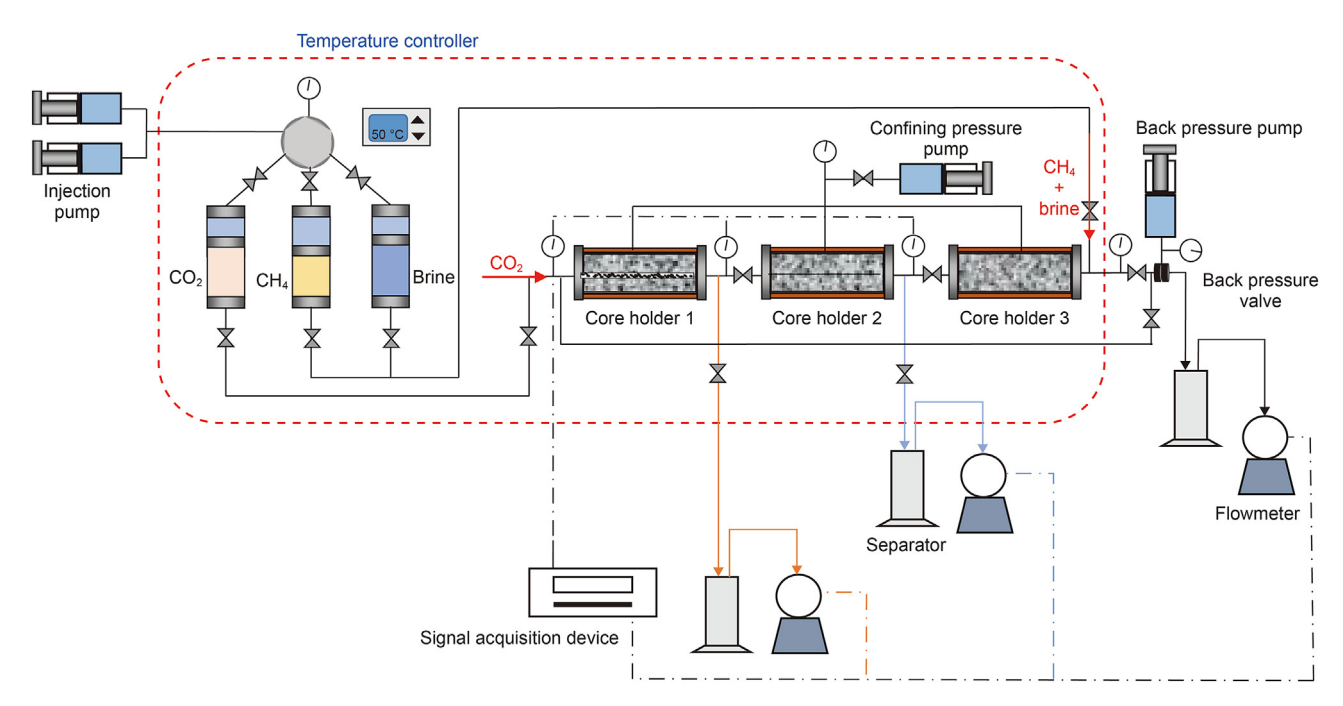


Fig. 3. Experimental device for CO<sub>2</sub> injection into coals.

1-4~mL/min for both the P1-F1-M1 and P2-F2-M2 coal sample combinations. The volume of  $CO_2$  injected into the P1-F1-M1 and P2-F2-M2 coal samples was the same, and the experiments were carried out under the same conditions.

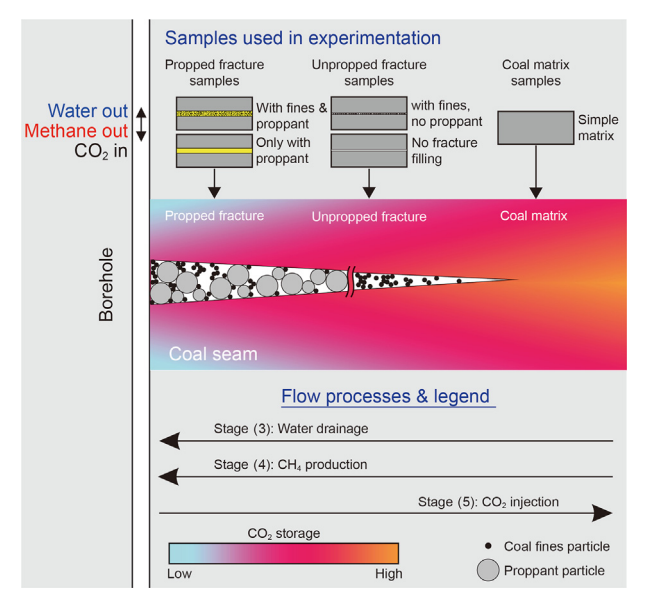
Following the experiment, the total volume of  $CO_2$  stored in the coal sample combination was released and measured. Finally, steps (1) to (5) were repeated. The multiple rounds of intermittent  $CO_2$  injection with equal time intervals were carried out after the first pressure decay stage. The total time of each subsequent round was 4 h and the injection time was 2 h, and the  $CO_2$  storage data for each subsequent round was calculated during the experiments.

Fig. 4 shows how the different types of samples represent various aspects of the fracture system in the coal seam, and how they are arranged relative to each other. The figure is arranged in the same direction as the core holders in Fig. 3, the coal containing the propped fracture on the left-hand side and the coal matrix on the right-hand side, with that containing the unpropped fracture between them. The figure also shows the flow of fluids in the subsurface as modelled in the experimental methodology (steps (3) to (5)). The coal fines are shown in the positions they would be occupying at the end of Stage II in Fig. 4 (step (3) of the experimental methodology). The coal seam is colour-coded according to the utilization of the maximum  $CO_2$  storage space. This schematic representation is based on our interpretation of the quantitative experimental data presented in the remainder of this paper.

# 3. Results and discussion

# 3.1. Migration and blockage of coal fines in fractures during drainage and CH<sub>4</sub> production stages

During the injection of water and subsequent flushing with CH<sub>4</sub>, the differential pressure across the sample changes as the relative permeability of the mobile fluid changes in response to their saturation and distribution. Fig. 5 shows the changes in injection pressure and the concentration of coal fines in the expelled fluid as a function of time during the water drainage and methane production stages of the core flooding for both the sample combination



**Fig. 4.** Schematic diagram relating the position and type of fractures in the experimentally modelled coal seam in relation to the sample types that are used to represent each part of the system arranged in the same direction as implemented in the experimental rig (Fig. 3). The large arrows represent flow processes occurring during each of the main stages of core-flooding, and the colour bar represents the utilization of the total  $CO_2$  storage capacity (schematically) based on the results described in this work.

containing coal fines and the sample combination without coal fines. As coals tend to be water-wet at low pressures but methanewet at high pressures (Mazumder and Wolf, 2008), we assume that the experimental conditions (confining pressure of 15 MPa and temperature of 50  $^{\circ}$ C) have rendered the sample methane-wet. In this case the initial injection of water represents a drainage process. This water drainage stage models the production of flowback water from the hydraulic fracturing.

In the drainage stages of the experiment, where water is being

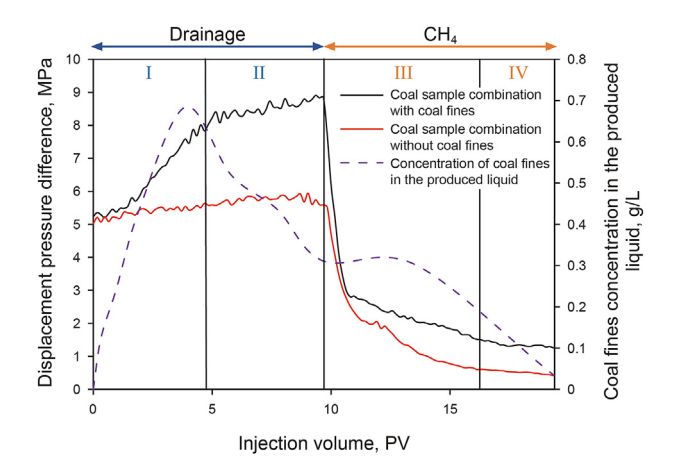


**Fig. 5.** Time evolution of water and  $CH_4$  injection pressure for coal sample combinations with coal fines (black solid line) and without coal fines (red solid line), together with the variation in coal fines concentration in the expelled fluid for the sample combination containing coal fines (purple dashed line). There was no expulsion of coal fines for the sample combination that contained no coal fines, and its curve is omitted as zero).

injected and flows through all three samples at  $P_{\rm conf}=15$  MPa and  $T=50\,^{\circ}{\rm C}$ , the progressive increase in injection pressure is governed by the reduction in water relative permeability. Subsequent injection of humidified methane leads to a rapid breakthrough and production of methane. The development of efficient gas flow pathways then leads to a significant drop in injection pressure and is associated with a continuous increase in the gas saturation in the coal pore and fracture space. The gas concentration in fluid becomes higher, and the corresponding displacement pressure difference decreases (due to the lower viscosity of gas). However, water continues to be produced with the gas stream, in small, and intermittent globules. As the water is removed from the core, the gas phase exhibits enhanced flow capability, resulting in a lower displacement pressure requirement.

For the sample combination that contained no coal fines (P2-F2-M2), no coal fines were expelled, and hence there was no associated curve in the figure. For this sample combination the injection pressure variation increased progressively but only by small amounts and was related solely to the varying gas and water relative permeabilities as saturation changed during the core flooding. The small-scale variation in injection pressure was related to the local-scale filling of voids in the sample until the sample was fully saturated.

For the sample combination that contained coal fines (P1-F1-M1), the same pressure behaviour was observed; however, the overall changes in pressure were greater. The increases in injection pressure during drainage were about approximately eight times higher. We attribute this to the mobilized water transporting the coal fines and which allows them to block the fracture. The coal fines were initially evenly distributed within the propped and unpropped fractures (as shown in Fig. 6(a)). In Stage I, the water filling the coal fractures begins to mobilise the coal fines, transporting them through the constrictions between proppant grains in the propped fracture and between the faces of the fracture itself in the case of the unpropped fracture. Some of these coal fines can become trapped at the restrictions, causing blockages. The accumulation of coal fines in the narrow restrictions affects the connectivity of the coal fracture space (Huang et al., 2017). As a consequence, the injection pressure rises rapidly. A large concentration of coal fines was measured in the output liquid (maximum value of 0.68 g/L) towards the end of Stage I at about 100 min,

which represents the peak of mobile coal fines production. This occurs just before a change in gradient of the increase in injection pressure, which was used to distinguish between Stage I and Stage II in the drainage process.

During Stage II, as the formation water continues to be injected, the injection pressure rises at a lower rate and the concentration of coal fines in the output fluid also decreases. The main reason is that the agglomeration and blockage of coal fines formed in Stage I gradually form a "coal fines filter cake" in Stage II. The coal fines filter cake is made of stable coal fines agglomerates, which are larger-scale and more compact coal fines blockages. The formation process of the coal fines filter cake is as follows: the fluid carrying coal fines subsequently flows through this area. As coal fines deposit in the constricted areas of the pores and fractures, the coal fines carried by the fluid aggregate with the deposited coal fines, creating an agglomerate with the ability to filter coal fines from the fluid (Zou et al., 2014; Bai et al., 2017). The filter cake is further compacted during the continuous water injection process (Fig. 6(b)), leading to a reduction in the amount of movable coal fines in the fractures and a reduction in the extent of coal fines migration. In addition, the coal fines filter cake acts as a filter for coal fines in the formation water, resulting in a decrease in the concentration of coal fines in the produced liquid. During this process, the volume of the coal fines filter cake gradually increases, and the injection pressure rises accordingly. The difference in injection pressure in the coal sample combinations with and without coal fines at this stage reflects the decrease in permeability of the coal sample combination after coal fines blockage.

Fig. 6 is a working model that contains a number of assumptions. Fig. 6(a) shows the assumed initial distribution of coal fines as being uniform. This is not an assumption because the experimental samples were constructed to initially have a uniform distribution of coal fines. Fig. 6(b) illustrates an assumption that coal fines have moved and aggregated into clusters capable of blocking flow pathways (shown diagrammatically in the figure). This was inferred from a number of experimental observations. First, coal fines were produced from the samples during drainage, showing the coal fines were mobile, but the expulsion of coal fines stopped before a considerable mass of them remained in the sample, indicating that water flow pathways had developed to an extent that by-passed the remaining, now immobile fines. That the remaining fines aggregated to block some flow pathways is supported by (i) the mutually attractive (aggregating) geochemistry of coal fines in brine solutions, (ii) the water flow streamlines, which would have transported the coal fines together to internal apertures, but above all (iii) the increase in flow pressure that occurred as aggregations of coal fines began to block apertures that would otherwise have remained open to flow. Once aggregated (Fig. 6(c) and (d)), the CO<sub>2</sub> flow depends on essentially a dual porosity system defined by two different grain sizes. In such a system the potential for cross-flow is greater because what would otherwise have been more direct flow pathways are made more tortuous by the presence of aggregations of coal fines that do not completely block apertures between proppant particles, but makes flow through them more contorted.

Once the sample combinations were fully saturated with water, methane was injected in the same direction. This step was carried out to model the production of natural methane from the coal gas resource. The fractures in the samples provide a very efficient pathway for the percolation of gas injected at high pressures. Consequently, the gas broke through the sample combinations quickly, and, once it has done so, forms efficient pathways for methane flow which require low injection pressures. Hence the methane relative permeability increased significantly. The gas injection pressure dropped rapidly in Stage III, and the concentration of coal fines in the produced liquid increased slightly at this time.

Q. Wang, Z.-J. Zhang, J.-L. Xiong et al. Petroleum Science 22 (2025) 2502-2515

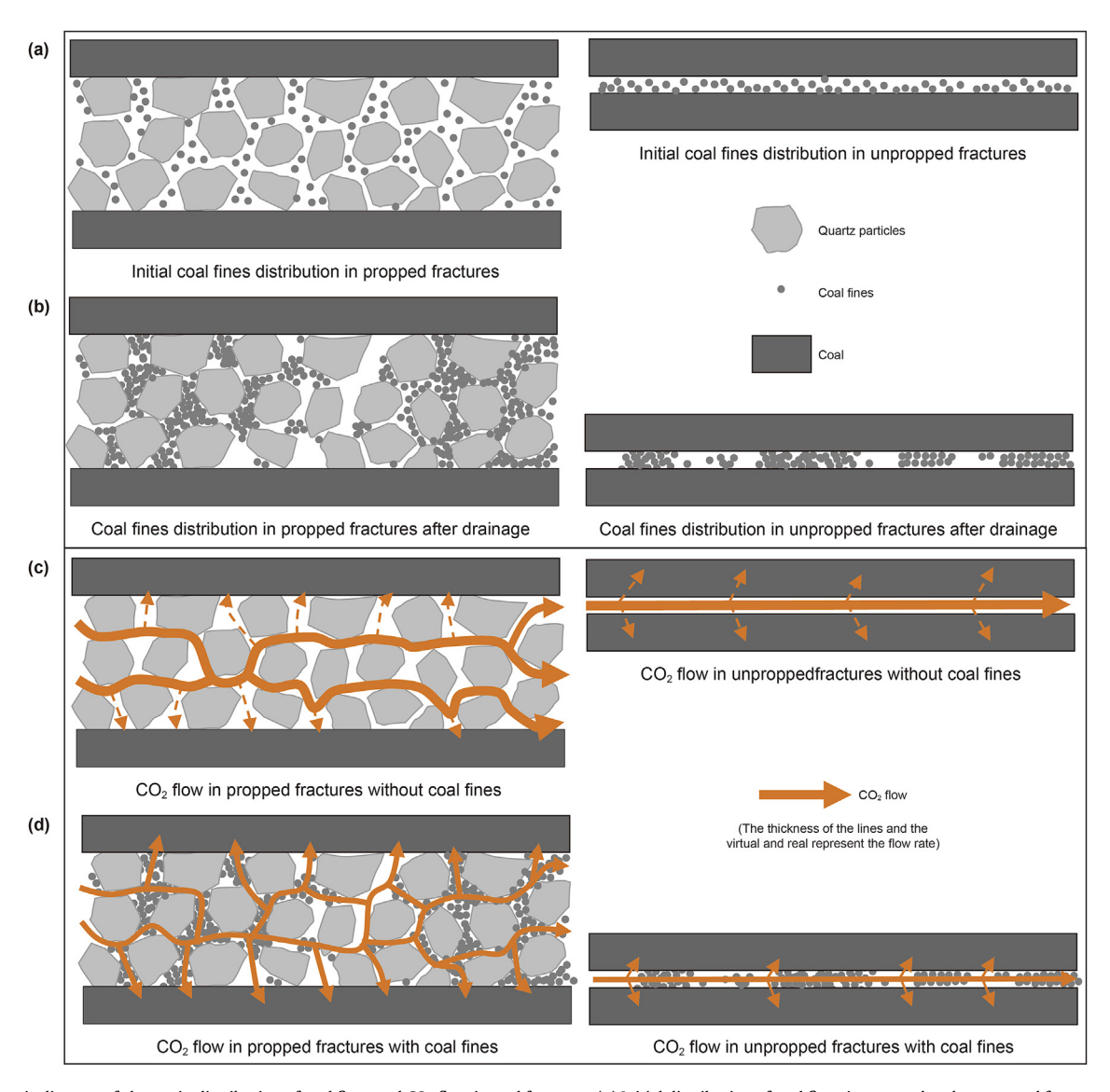


**Fig. 6.** Schematic diagram of change in distribution of coal fines and CO<sub>2</sub> flow in coal fractures. (**a**) Initial distribution of coal fines in propped and unpropped fractures, (**b**) assumed distribution of coal fines after drainage, (**c**) flow of CO<sub>2</sub> in propped and unpropped fractures with no coal fines, (**d**) flow of CO<sub>2</sub> in propped and unpropped fractures with the presence of coal fines.

The gas—water two-phase flow was able to break down some of the aggregations of coal fines, remobilizing them and allowing them to be produced. There are differences in the ability of fluids with varying gas-to-water ratios to initiate the migration and carry coal fines. The water phase has a strong ability to carry and transport coal fines. However, when the fluid was a mixture of gas and water, the disturbance effect on coal fines during flow (interfacial effect) is stronger, which can re-initiate the deposited coal fines and carry them away with the fluid again (Huang et al., 2024; Zhu et al., 2017). It would be expected that the presence of remobilized coal fines in the production fluids would likely lead to higher injection pressures than would otherwise be expected. This is likely to be the case for Stage III, because after the second peak in coal fines concentrations in the expelled fluids which occurred at approximately 400±60 min, the injection pressures dropped swiftly in Stage IV. In Stage IV, the output liquid volume was only 3.1 mL, which was 15.5% of that in Stage III (20.67 mL).

Towards the end of Stage IV of the experiment, a stable water

saturation had been established, with progressively less water being produced and a relative permeability of water approaching zero. The water saturation was approximately 29.8% with coal fines and 26.6% without coal fines, calculated based on the volume of injected and produced water. Although by the end of Stage IV, the coal had retained some immobile water, this does not represent an irreducible water saturation in the conventional sense because the sample is gas-wet. Since coal fines are transported in the water phase rather than the gas phase due to the higher density and viscosity of water, production of coal fines falls to almost zero by the end of Stage IV (Danso et al., 2021). However, the sample combinations still contain significant coal fines blockages.

At this stage in the experiment, the storage of water in the coal seam had been modelled together with the subsequent production of methane from the propped and unpropped fractures and matrix within the coal seam. The next step in the experiment was to model the injection of CO<sub>2</sub> into the coal seam through the injection of CO<sub>2</sub> through the core combinations in the opposite direction.

In this step (experimental step (5)), the process of  $CO_2$  storage had been modelled, the gas  $CO_2$  was injected sequentially from the left-hand side of each core, in such a way that the propped fracture experienced the  $CO_2$  first, flowed by the unpropped fracture and finally the unfractured rock matrix. The differential pressure changes during this process were negligible essentially because methane was being replaced by  $CO_2$  in the same gas-filled channels. This step was, however, critical for the science reported in this paper, as we aimed to ascertain the efficiency of  $CO_2$  storage for legacy coal beds that have previously been exploited for methane and the effects of coal fines on the processes. It should be noted that the reverse flow of injected  $CO_2$  is highly likely to cause the remigration of coal fines during the  $CO_2$  injection process, although the ability of a single gas-phase fluid to carry coal fines is relatively weak.

After the core flooding experiments, the cores were cut into four equal parts and ground to a powder. Post-core flooding tests (experimental step (6)) were carried out on the cores to characterize the degree of migration of coal fines along the direction of  $CO_2$  injection by liberating the remaining coal fines in each subsample using a fixed volume of water and analyzing the concentration of coal fines in the resulting solution. Fig. 7 shows the relative concentration of coal fines remaining in the solutions prepared from the core material from each of four sections of the core sample, relative to the value at the  $CO_2$  injection end of the sample (water flow output end).

The concentration of coal fines in the solution was highest for the material nearest to the CO<sub>2</sub> injection face of the sample for both the propped and unpropped fractures. The concentration of coal fines in the solution decreased monotonically with increasing distance from the CO<sub>2</sub> injection face for both types of fractures, with the greater reduction occurring for the unpropped fracture.

These data suggest that a build-up of aggregated coal fines filter cake by the initial drainage remaining after the  $\mathrm{CO}_2$  injection phase of the experiment has occurred. Such an interpretation implies that the subsequent reverse injection of  $\mathrm{CO}_2$  does not change the overall distribution trend of coal fines in the fractures resulting from water movement.

Furthermore, the more pronounced variation in coal fines across the samples in the unpropped fracture indicates that the presence of the quartz proppant grains has impeded the transport of coal fines through the fracture, resulting in a coal fines distribution that deviates from its initially uniform state, but without concentrating the coal fines as strongly toward the water flow output end as in the unpropped fracture, where no impeding mechanism is present.

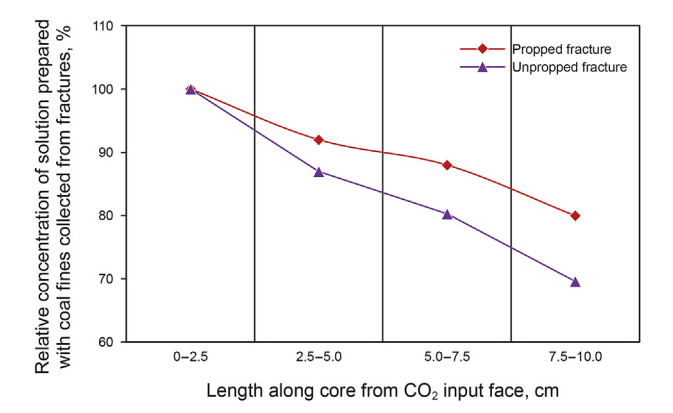


**Fig. 7.** Distribution of coal fines in fractures after CO<sub>2</sub> injection, represented by the concentration of coal fines in a solution made with equal amounts of solvent.

3.2. Characteristics and mechanism of CO<sub>2</sub> storage in coal and the effect of coal fines

The  $CO_2$  storage characteristics through reverse  $CO_2$  injection into the coal sample combinations containing propped and unpropped fractures, and the matrix, both with and without coal fines, after drainage and methane gas production, were investigated. The results are shown in Figs. 8 and 9. Fig. 8 shows  $CO_2$  storage for each sample within the sample combinations with and without coal fines, as well as the difference in their  $CO_2$  storage potential.

The CO<sub>2</sub> storage is highest in the coal matrix, at 30.7 and 33.6 cm<sup>3</sup>/g for the two matrix samples. Neither of these matrix samples was loaded with coal fines, nor could have had coal fines flow into them during the drainage or methane production stages of the experiment. Consequently, their difference represents only a natural variation between the samples. It is worth noting that these values are just over half that expected from the maximum CO<sub>2</sub> storage capacity measurements that were discussed above and shown in Fig. 2. The reason for this is that the maximum CO<sub>2</sub> storage measurements are for fully stabilized storage of CO<sub>2</sub> in a CO<sub>2</sub>-saturated system. The core-flooding experiments are dynamic flow measurements in which the CO<sub>2</sub> had not reached stable saturation, finishing 13.1 h after the commencement of injection, not when full sorption has occurred but only when the chromatograph showed no more methane present in the system.

The CO<sub>2</sub> storage amount of matrix coal without coal fines is 14.6 and 11.9 cm<sup>3</sup>/g, respectively, higher than that of propped fractured and unpropped fractured coal. The difference is 10.8 and 5.4 cm<sup>3</sup>/g under the conditions of containing coal fines. This is because the propped and unpropped fractured coal samples have such high fluid conductivities that gas channeling seriously reduces the CO<sub>2</sub> storage effect. In other words, CO<sub>2</sub> breakthrough occurs very quickly and thereafter CO<sub>2</sub> bypasses the surrounding rocks rather than entering them for storage.

In fractured coal, the amount of  $CO_2$  that enters the fracture wall and is adsorbed and stored by the matrix part is small (Fig. 6(c)). Diffusion in this process is the main way for  $CO_2$  to transfer mass to the matrix part of fractured coal. The fractures, as high-permeability channels, shield the matrix part. As a result, coal has a limited ability to capture  $CO_2$ , and simultaneously reduces the  $CO_2$  storage fraction and  $CO_2$  storage capacity. In downstream matrix coal with a relatively homogeneous pore throat structure, the displacement pressure causes  $CO_2$  to enter more pores, where convective mass transfer plays a major role. Hence,  $CO_2$  has a high efficiency in replacing  $CH_4$  and being adsorbed by coal. However,

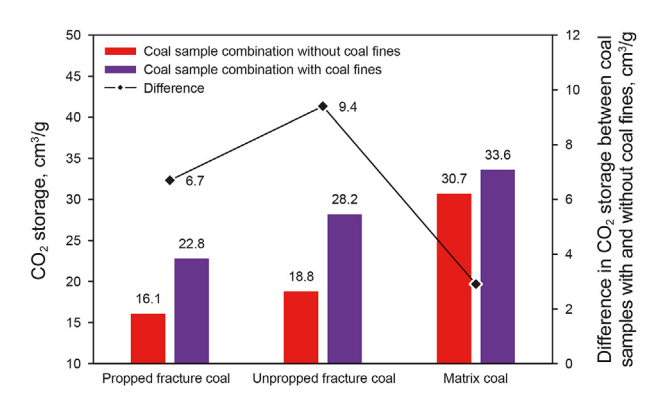


**Fig. 8.** CO<sub>2</sub> storage characteristics of coal sample combinations containing propped and unpropped fractures and matrix coal.

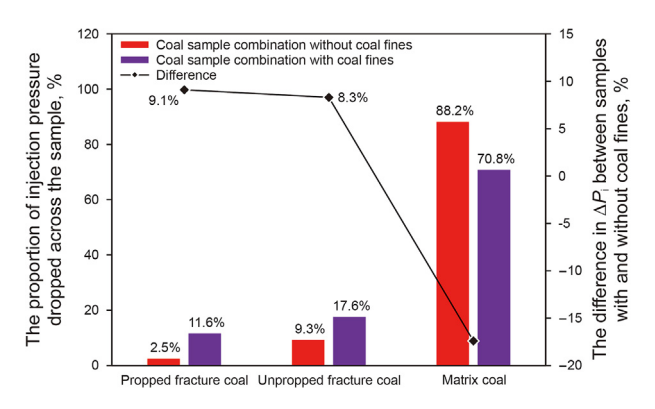


**Fig. 9.** Characteristics of  $CO_2$  injection pressure difference ( $\Delta P_i$ ) dropped across propped, unpropped, and matrix coal samples.

there is no such displacement pressure difference in coal with fractures, which drives CO<sub>2</sub> through the fracture wall to the matrix part where it is stored (Li et al., 2022).

Fig. 9 shows the percentage of the total gas injection pressure drop across the propped (< 12%) and unpropped (< 18%) fractures was very small. This is due to the formation of gas channels which efficiently transport the gas through the fracture systems. Most of the injection pressure drop occurs across the matrix coal (88.2% and 70.8%). Consequently, the high gas pressure difference occurring in the coal matrix facilitates a greater volume of  $CO_2$  to enter a wider range of pores there. As before, the difference in the matrix values arises from natural variation within the rocks themselves rather than from the variation in coal fines content.

In addition, it is worth noting that the role of fractures in the process of methane production and CO<sub>2</sub> injection in the coal seam is different. Multiple wells in a coal seam produce methane simultaneously, and the hydraulic fracturing network system is a high-permeability channel for the CH<sub>4</sub> desorption from the coal seam matrix to flow smoothly to the wellbore, and there is no adverse factor for production. However, when CO<sub>2</sub> is injected into the coal seam, the flow field between the injection and production wells is primarily governed by the hydraulic fractures. The fractures are both a channel for CO<sub>2</sub> to flow to the coal seam matrix part, and also cause the injected CO<sub>2</sub> to flow directly and quickly to the production well. Moreover, the resistance to CO<sub>2</sub> entering the matrix from the fracture is significantly higher than that of CO<sub>2</sub> flowing along the fracture to the production well, resulting in a large amount of injected CO<sub>2</sub> not being effectively stored in the matrix part. Therefore, gas channeling is the most common problem of CO<sub>2</sub> injection in fractured reservoirs, and it is also the key to determine whether the CO<sub>2</sub> injection production and storage measures can be successfully implemented.

Blockage of high-permeability channels may be an effective measure (Lv et al., 2020). The coal fines blocking the fractures during the drainage and gas production stage play a role in increasing the fluid flow resistance in the propped and unpropped fractures, increasing the injection pressure drop across them, hence inhibiting gas channeling and improving the  $\rm CO_2$  storage effect of fracture coal seams.

Evidence for the efficacy of fracture plugging to improve  $CO_2$  storage in coal samples containing propped and unpropped fractures can be found in our data. Examination of the difference in  $CO_2$  storage between coal samples with and without coal fines in Fig. 7 shows that samples which contained coal fines were associated with greater  $CO_2$  storage. For propped fractures, the  $CO_2$  storage value was  $22.8 \text{ cm}^3/\text{g}$  for fractured samples with occluding coal fines, compared with  $16.1 \text{ cm}^3/\text{g}$  for the sample without coal fines,

representing a storage increase of  $6.7 \text{ cm}^3/\text{g}$ , or 41.6%. For unpropped fractures, the  $CO_2$  storage value was  $28.2 \text{ cm}^3/\text{g}$  for fractured samples with occluding coal fines, compared with  $18.8 \text{ cm}^3/\text{g}$  for the sample without coal fines, an increase of  $9.4 \text{ cm}^3/\text{g}$ , or an improvement of 50%.

As we have already mentioned, the efficiency of CO<sub>2</sub> flow through the propped and unpropped fractures results in little if any of the CO<sub>2</sub> percolating into the coal matrix each side of the fracture. This is the situation shown by the purple to orange colour-coding in Fig. 4. The blocking or partial occlusion of propped and unpropped fractures allows the CO<sub>2</sub> more time to enter the neighbouring coal matrix through convective mass transfer (Fig. 6(d)), increasing the contact time and area between the coal matrix bordering the fractures, allowing CO<sub>2</sub> to be captured, fully adsorbed and stored. Hence partial fracture occlusion by coal fines has the dual effect of (i) enhancing CO<sub>2</sub> storage in the coal matrix bordering the fractures, while (ii) reducing access of CO<sub>2</sub> to the unfractured matrix deeper in the coal seam. (The fractures are blocked by coal fines, which hinders the injection of CO<sub>2</sub> into the matrix coal further away from the well, increasing the difficulty of CO<sub>2</sub> injection). These two effects would need to be controlled and balanced in order to optimise CO<sub>2</sub> injection and storage.

The overall CO<sub>2</sub> storage characteristics of both coal sample combinations (i.e., with and without coal fines) are shown in Table 3. Due to the coal fine blockage in the fractures, the overall permeability of the coal sample combination decreases, and under the same injection pressure difference, it takes a longer time to inject the same volume of CO<sub>2</sub>, which increases the cost of CO<sub>2</sub> injection. However, it also increases the interaction time between the injected CO<sub>2</sub> and the coal seam, which makes the total CO<sub>2</sub> storage amount, the utilization degree of CO<sub>2</sub> storage potential, the CO<sub>2</sub> storage fraction, and the CH<sub>4</sub> recovery rate of the coal sample combination all increase significantly. The increased CH<sub>4</sub> recovery rate suggests that a greater amount of CH<sub>4</sub> in the pore space is being displaced by CO<sub>2</sub>, accompanied by a notable expansion in the swept volume during CO<sub>2</sub> injection.

Consequently, after hydraulic fracturing, the coal fines remaining in the coal fractures after the drainage and gas production stages play a significant role, blocking the fractures and delaying the breakthrough of CO<sub>2</sub>. However, since the fractures also retain a certain conductive capacity, the injectivity of the coal seam is maintained, and the slowing of CO<sub>2</sub> flow can have an overall beneficial effect on CO<sub>2</sub> storage (Liu et al., 2020).

In summary, although coal fines blockage in fractures increases the difficulty and cost of  $CO_2$  injection, it mitigates the negative impact of gas channeling in the hydraulic fracturing network system on  $CO_2$  storage, and increases the feasibility of  $CO_2$  storage by injecting  $CO_2$  into hydraulically fractured coal seams. Since the presence of coal fines has a significant effect on the flow and storage of  $CO_2$ , its effect on  $CO_2$  injection parameters should be taken into account when judging the feasibility of  $CO_2$  storage by injecting  $CO_2$  into coal seams with coal fines.

# 3.3. Effect of injection parameters on CO<sub>2</sub> storage effect in coal under coal fines constraint

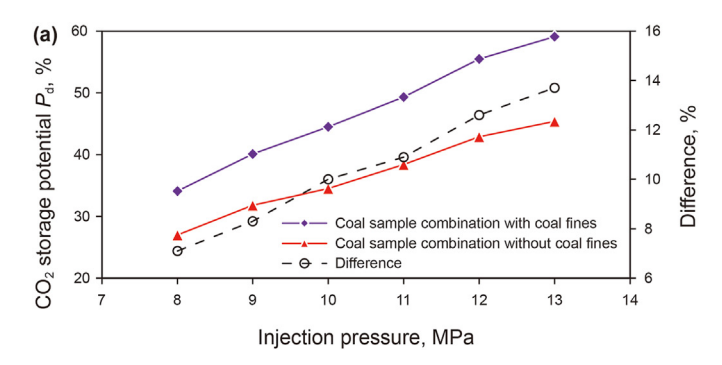
The pressure of  $CO_2$  injection has a significant effect on the  $CO_2$  storage effect in coal at the same temperature conditions (Fan et al., 2021). When the injection pressure increases from 8 to 13 MPa with the same injection pressure difference, the  $CO_2$  storage potential and  $CO_2$  storage fraction of the coal sample combination with coal fines increase by 25.0% and 18.4%, while those of the sample combination without coal fines increase by 14.1% and 7.2%, respectively. The full data is shown in Fig. 10.

The ability of coal to store CO<sub>2</sub> increases as the injection pressure

**Table 3** CO<sub>2</sub> storage characteristics of coal combinations.

| Coal sample combination | Injection time, h | Injection volume, L | $S_{\rm p}$ , cm <sup>3</sup> /g | $P_{\rm d},\%$ | F, % | CH <sub>4</sub> recovery rate, % |
|-------------------------|-------------------|---------------------|----------------------------------|----------------|------|----------------------------------|
| Without coal fines      | 10.6              | 51.2                | 21.9                             | 34.6           | 35.7 | 45.9                             |
| With coal fines         | 13.1              | 51.2                | 28.4                             | 44.5           | 47.5 | 67.8                             |
| Difference              | 2.5               | 0                   | 6.5                              | 9.9            | 8.8  | 21.9                             |

Notes: Injection volume was measured at 25 °C and 0.1 MPa.



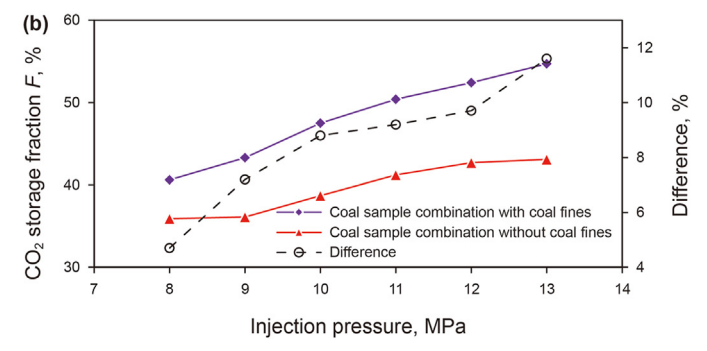


Fig. 10. Influence of injection pressure on CO<sub>2</sub> storage effect in coal sample combinations with and without fines. (a) CO<sub>2</sub> storage potential P<sub>d</sub>, (b) CO<sub>2</sub> storage fraction F.

increases because the higher pressures allow  $CO_2$  to enter a larger range of micropores, accessing the smaller pores which are difficult to fill at the lower pressures. The ability of the coal to adsorb  $CO_2$  also increases as pressure increases, enhancing the  $CO_2$  storage potential as well as ensuring that the amount of  $CO_2$  stored per amount of  $CO_2$  injected (i.e., the  $CO_2$  storage fraction) will also increase.

The injection pressure effect is more pronounced for samples that contain coal fines than for those which do not contain coal fines (Fig. 10). The presence of coal fines leads to a higher flow resistance, which thereby increasing the time required to inject the same amount of CO<sub>2</sub>. Indeed, the samples containing coal fines took 1.1–2.8 h longer than the samples without coal fines at the same injection volume. This can be seen clearly in Table 4. The prolonged injection time results in higher injection costs. Moreover, the difference between CO<sub>2</sub> storage potential values for coal sample combinations with and without coal fines also increases as the injection pressure increases (Fig. 10(a)). A similar trend is observed for the CO<sub>2</sub> storage fraction (Fig. 10(b)). These data indicate that the presence of coal fines improves both the CO<sub>2</sub> storage potential and storage fraction.

One factor contributing to the pressure differences is the fracture aperture. Under constant overburden pressure, increasing the injection pressure leads to fracture opening and easier CO<sub>2</sub> injection. The presence of coal fines facilitates this process while also inducing a greater degree of flow heterogeneity in the sample, reducing CO<sub>2</sub> gas channeling.

The CO<sub>2</sub> storage potential and CO<sub>2</sub> storage fraction are also

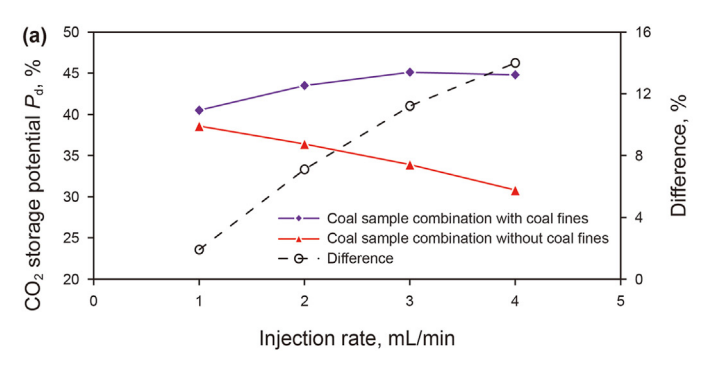
**Table 4**Difference in injection time of coal sample combinations with and without coal fines

| Injection pressure, MPa | Total injection time               | Difference, h |     |
|-------------------------|------------------------------------|---------------|-----|
|                         | Without coal fines With coal fines |               |     |
| 8                       | 8.4                                | 9.5           | 1.1 |
| 9                       | 9.9                                | 11.8          | 1.9 |
| 10                      | 10.6                               | 13.1          | 2.5 |
| 11                      | 12.1                               | 14.9          | 2.8 |
| 12                      | 12.6                               | 15.3          | 2.7 |
| 13                      | 12.1                               | 14.3          | 2.2 |

affected by the injection rate, as shown in Fig. 11. However, the relationship is more complex. As the injection rate increases, there is a slight increase in CO<sub>2</sub> storage potential and CO<sub>2</sub> storage fraction for the samples containing coal fines. However, in contrast, these parameters decrease significantly with increasing injection rate in samples without coal fines. In this work the injection rate was varied from 1 to 4 mL/min. Over this range of injection rates, the CO<sub>2</sub> storage potential and CO<sub>2</sub> storage fraction of the samples with coal fines increase by 4.3% and 3.3%, respectively, whereas in samples without coal fines, these values decrease by 7.8% and 4.4%.

As the injection rate increases, the flow heterogeneity effect of the coal sample combination becomes more significant (Wang et al., 2019), with CO<sub>2</sub> gas channeling becoming more significant, and the CO<sub>2</sub> content in the produced gas reaching a higher value more rapidly. This is an indication of a decrease in the CO<sub>2</sub> storage fraction, indicating that the coal seam is not fully capturing and adsorbing the injected CO<sub>2</sub>. However, the coal fines blockages in the fractures can reduce the effect of increased gas channeling caused by the increase in injection rate. On the other hand, a higher injection rate corresponds to the larger injection pressure, and the larger CO<sub>2</sub> injection rate may cause the coal fines to migrate again. Although the gas flow has a limited ability to disturb and carry coal fines, the CO<sub>2</sub> injection pressure is generally higher than the pressure of coal seam fluid. Such high injection pressure inevitably affects the distribution of coal fines in fractures (Han et al., 2021; Huang et al., 2021). Under the combined influence of these factors, the CO<sub>2</sub> storage of the coal sample combination with coal fines increases slightly with the increase in injection rate. Therefore, when carrying out CO<sub>2</sub> storage in coal seams which contain a large amount of coal fines, the CO<sub>2</sub> injection rate can be appropriately increased, which can improve the CO<sub>2</sub> injection efficiency without causing a large negative impact on CO<sub>2</sub> storage. However, it is worth noting that the maximum injection pressure difference when coal fines are present is 0.5–2.1 MPa higher than that without coal fines for the same injection volume (Table 5), which significantly increases the difficulty of CO<sub>2</sub> injection.

In summary, the coal fine blockage in the fractures mitigates the negative impact of the increases in injection pressure and injection rate on the  $CO_2$  storage effect of hydraulic fractured coal seam, but at the same time increases the time and difficulty of  $CO_2$  injection. The



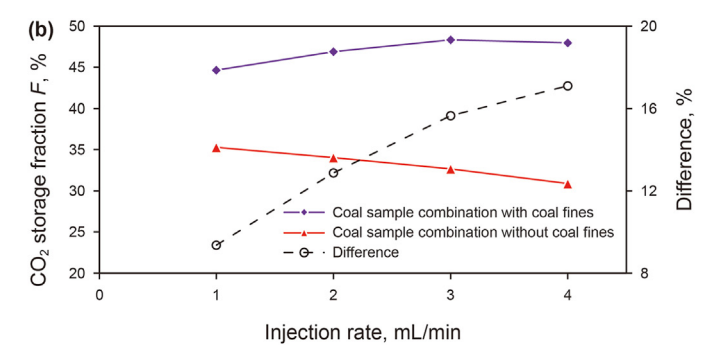


Fig. 11. Influence of injection rate on CO<sub>2</sub> storage effect in coal sample combinations with and without fines. (a) CO<sub>2</sub> storage potential P<sub>d</sub>, (b) CO<sub>2</sub> storage fraction F.

**Table 5**Difference in injection pressure of coal sample combinations with and without coal fines.

| Injection rate, mL/min | Maximum injection pressure difference, MPa |                 | Difference, MPa |
|------------------------|--|-----------------|-----------------|
|                        | Without coal fines                         | With coal fines |                 |
| 1                      | 1.1  | 1.6             | 0.5             |
| 2                      | 1.8  | 2.9             | 1.1             |
| 3                      | 2.6  | 4.4             | 1.8             |
| 4                      | 3.8  | 5.9             | 2.1             |

difficulty of  $\mathrm{CO}_2$  injection could be reduced and the  $\mathrm{CO}_2$  storage effect in the coal seam could be further improved by adjusting the injection mode while maintaining higher injection pressure and rate.

# 3.4. The effect of intermittent injection on CO<sub>2</sub> storage in coal

The coal pore space continues to adsorb  $CO_2$  significantly after injection stops. This leads to a significant drop in gas pressure after injection has ceased. This effect is due to a combination of flow heterogeneity in the coal sample combination, which causes  $CO_2$  gas channeling during the injection process, and the long time required for full  $CO_2$  adsorption in the coal matrix. Fig. 12 shows the decay in pore gas pressure after  $CO_2$  injection at 10 MPa and 50 °C has been stopped.

In general, all curves decrease rapidly for the first 1000 min, followed by a progressively more gradual decrease until the end of the experiment at 4000 min. The early time behaviour can be modelled by an exponential decay. The shape of the curves depends

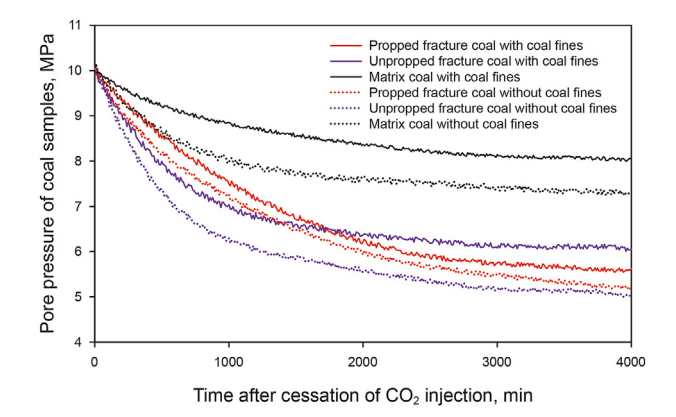


**Fig. 12.** Pressure decay curves for coal samples containing propped fractures and unpropped fractures and matrix coal sample after cessation of  $CO_2$  injection at back pressure of 10 MPa and 50 °C, together with appropriate exponential fits.

on both the decrease in the  $CO_2$  adsorption rate, and the rate of pressure decrease as the pressure decreases. The decay is exponential because exponential relationships arise when a parameter's value is dependent on its previous state. Here, the gas pressure in the pores decreases because the gas is being adsorbed by the coal, while simultaneously the efficiency of gas adsorption depends on the gas pressure (the higher the gas pressure, the higher the adsorption).

For the samples without coal fines, when compared under the same conditions, the pressure decay of the matrix sample is the slowest, followed by the propped fracture, while the unpropped fracture exhibits the fastest pressure drop. This order reflects the increasing mobility of  $CO_2$  within the sample, as expected. For the samples with coal fines, the pressure decay is slower than the corresponding case in which the samples contain no fines. This is expected, as coal cores containing coal fines have already absorbed more  $CO_2$  than those without coal fines during  $CO_2$  injection, the efficiency of coal cores continuing to adsorb  $CO_2$  is lower at higher  $CO_2$  adsorption volumes. However, the later decay becomes a little more complex in that the early decay exhibited by the unpropped fracture with fines ceases prematurely, while the propped fracture maintains a continuous pressure decline, hence changing the order of the data

Exponential curves have been fitted to the early-time pressure data. These are shown in Fig. 12, where the data are shown as solid lines for samples with fines and dots for sample without fines and the exponential fits are given by dashed lines, so that they can be seen more easily. The fitting equation is

$$P_{\text{pore}} = A + (P_0 - A)\exp\{-Bt\},\tag{4}$$

where  $P_{\rm pore}$  is the gas pressure (on the *y*-axis of Fig. 12), MPa; *t* is the elapsed time (*x*-axis), min; *A* is a fitting coefficient, MPa; *B* is a second fitting coefficient, min<sup>-1</sup>, and the corresponding time constant is defined as the reciprocal of *B*, min. The data for these fits are shown in Table 6.

The functional form of the decay, as given in Eq. (4), is exponential, which agrees well with the expected exponential decay for transient mass flow through a porous medium where the input

**Table 6** Exponential fitting parameters for the data in Fig. 12.

| Core                             | A, MPa | B, min <sup>-1</sup>  | Time constant, min |
|----------------------------------|--------|-----------------------|--------------------|
| Matrix with fines                | 8.05   | $9.8 \times 10^{-4}$  | 1020               |
| Matrix without fines             | 7.35   | $13.5 \times 10^{-4}$ | 741                |
| Unpropped fracture with fines    | 6.10   | $15 \times 10^{-4}$   | 667                |
| Unpropped fracture without fines | 5.50   | $18 \times 10^{-4}$   | 556                |
| Propped fracture with fines      | 5.30   | $7.5 \times 10^{-4}$  | 1333               |
| Propped fracture without fines   | 5.15   | $8.9 \times 10^{-4}$  | 1124               |

Q. Wang, Z.-J. Zhang, J.-L. Xiong et al. Petroleum Science 22 (2025) 2502—2515

pressure decays as a result of the flow process. In this format, the initial gas pressure is  $P_0$  (MPa), where  $P_0 = 10$  MPa for all measurements in this work. The coefficient A represents the asymptotic pressure to which the pressure falls at long duration. The coefficient B represents the time constant, which governs the speed of the decay. Larger values of B increase the approach of the pressure to its asymptote. Halving the value of B doubles the time taken for the pressure to reduce to any specific value between  $P_0$  and A.

The coefficients A and B are linked and should be interpreted jointly. This is because a certain pressure  $P_{\rm pore}$ , where  $P_{\rm o} > P_{\rm pore} > A$ , can be obtained from an infinite set of pairs of (A, B) data forming a pair of continuous functions A = f(B) and B = f(A), which both also depend on  $P_{\rm o}$ . However, they are linked mathematically, the coefficients A and B carry their own independent physical information. The coefficient A carries information about the lowest pore gas pressure that can be physically attained during equilibration of gas where no additional gas is being injected, and B carries information about how quickly a certain degree of equilibration can be reached.

Referring to Table 6, the unpropped fracture with coal fines exhibited a rapid trend of pressure decay, while got a higher final pore pressure compared to the propped fracture with coal fines. This is because the volume of unpropped fracture space is smaller than that of propped fracture space. Assuming that CO<sub>2</sub> continues to be absorbed by the same volume in the initial stage, the gas pressure in the unpropped fracture space decreases more rapidly than that in propped fracture space. The unpropped fracture core stored more CO<sub>2</sub> after the experiment than propped fracture cores (refer to Figs. 8 and 9). Consequently, the unpropped fracture core has limited ability to continue absorbing CO<sub>2</sub> during the pressure decay stage after the experiment, resulting in a higher residual CO<sub>2</sub> pressure in the fracture space.

It was recognised that the first injection did not effectively exploit the CO<sub>2</sub> storage potential of the coal seam using the experimental parameters. We hypothesize that it would be possible to improve the performance by extending the CO<sub>2</sub> injection duration. However, we have chosen to implement a CO<sub>2</sub> "soaking" stage instead. This process involves stopping CO<sub>2</sub> injection and shutting the well in. Such a technique has been found to aid hydrocarbon production in CO<sub>2</sub>-enhanced oil recovery (EOR) processes (Wang Q. et al., 2021, 2022a, 2022b).

The implementation of multi-round  $CO_2$  injection and soaking implemented in this work used 5 rounds where each round of  $CO_2$  injection was stopped after 120 min. Cessation of injection was followed by pressure decay during which there were 120 min of shutin before the subsequent round. The  $CO_2$  storage characteristics of the coal sample combination with multiple rounds of equal time intermittent injection after the first injection at 50 °C and 13 MPa are shown in Figs. 13 and 14.

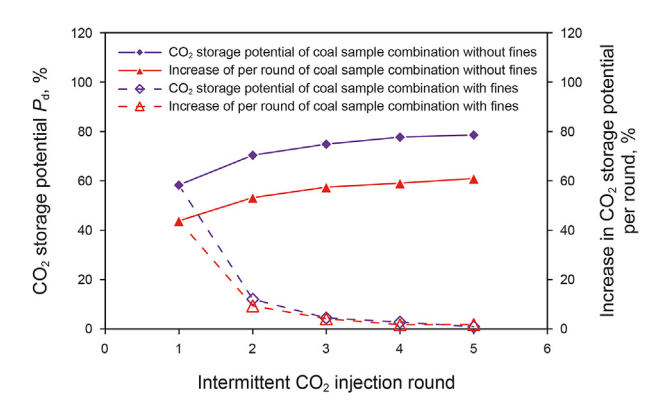


**Fig. 13.** The  $CO_2$  storage potential  $P_d$  of coal sample combinations with and without fines during 5 rounds of intermittent  $CO_2$  injection each followed by a shut-in period.

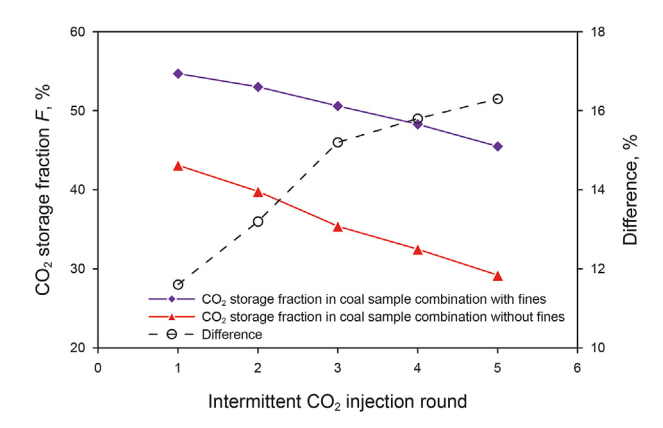


**Fig. 14.** The CO<sub>2</sub> storage fraction *F* in coal sample combinations with and without fines during 5 rounds of intermittent CO<sub>2</sub> injection each followed by a shut-in period.

Fig. 13 shows that the CO<sub>2</sub> storage potential of the coal sample combinations with and without coal fines can reach 78.6% and 60.9% after 5 rounds, respectively, which is 20.4% and 17.1% higher than that of the first injection of CO<sub>2</sub>. Fig. 13 clearly shows that CO<sub>2</sub> storage is improved for the sample combinations without and with fines, and roughly to the same degree. It is interesting to note that the improvement of CO<sub>2</sub> storage decreases after the first couple of rounds for the sample combinations with and without fines, leaving the sample without fines to retain a better overall storage potential even after five rounds of injection and soaking. It is no surprise that it becomes increasingly difficult to store more CO<sub>2</sub> in a reservoir which is progressively being filled, and has less and less accessible space to do so, but has the consequence that it is unlikely that 3 or more rounds would be economically justified in reality.

One would expect the  $CO_2$  storage fraction to decrease for subsequent rounds. This is shown in Fig. 14. The  $CO_2$  storage fractions in the coal sample combinations with and without coal fines decrease by 9.2% and 13.9% after 5 rounds, respectively, based on the first  $CO_2$  storage, as expected. However, the difference in  $CO_2$  storage fraction between the coal sample combinations with and without coal fines increases as the rounds increase. This result indicates that the coal fines blockage impedes gas flow sufficiently for more  $CO_2$  to be stored than when no fines are present. This effect can partially alleviate the decline trend of  $CO_2$  storage fraction in the subsequent rounds of injection.

The "n-Round Injection-Soaking CO $_2$ " (nRIS) method described above can be adapted according to the pressure decay characteristics of each round. It is not necessary to wait for the pressure to decay to a stable level before starting injection again. Indeed, the optimal approach may be restart injection of CO $_2$  after the rapid pressure decay stage is over, and to stop CO $_2$  injection immediately when the coal seam pressure recovers to the pressure of the first injection. Such a protocol would reduce the difficulty of CO $_2$  injection, shorten the intermittent injection time, and improve the CO $_2$  storage fraction.

Based on the results of this study, it is recommended that early pressure decay data is logged and an exponential curve is fitted to the decay. Soaking should be stopped, and a new injection should begin after a soaking time equal to the exponential decay time constant in Eq. (4).

# 4. Conclusions

Experiments were conducted to simulate the water drainage, methane production, and subsequent CO<sub>2</sub> injection in hydraulically fractured coal seams. Experiments were conducted with samples

with and without coal fines and for single CO<sub>2</sub> injections as well as intermittent multi-round CO<sub>2</sub> injections separated by CO<sub>2</sub> "soaking" periods.

During the drainage stage, the migration and blockage of coal fines in the coal fractures caused the resistance to fluid flow to increase rapidly by 51.9%, and the coal fines concentration in the produced liquid decreased rapidly by 54.4% after the formation of a stable "coal fines filter cake". The single-phase gas flow carrying capacity of coal fines was weak during the gas production stage.

The total CO<sub>2</sub> storage capacity and storage fraction of the coal with coal fines were 6.5 cm<sup>3</sup>/g and 8.8% higher than that without coal fines, respectively. Coal fines increased the CO<sub>2</sub> storage capacity of fractured coal by the largest margin, which was 9.4 cm<sup>3</sup>/g.

The increase in injection pressure increased the  $\rm CO_2$  storage potential and  $\rm CO_2$  storage fraction in coal with coal fines by 25.0% and 14.1%, respectively, which were 6.6% and 6.9% higher than that without coal fines, respectively. The increase in injection rate slightly improved the  $\rm CO_2$  storage fraction in coal with coal fines, but the  $\rm CO_2$  storage potential of coal without coal fines decreased significantly by 7.8%.

Multiple rounds of intermittent injection of  $CO_2$  could continue to exploit the  $CO_2$  storage ability of fractured coal by 20.4% if coal fines were present, or 17.1% with no coal fines, but the improvement of each subsequent round decreased rapidly from 12.1% for Round 2, to 1.7% after Round 5.

The coal fines retained in the fractures increased the CO<sub>2</sub> injection time by 1.1–2.8 h or the injection pressure difference by 0.5–2.1 MPa. Meanwhile, they reduced the effect of gas channeling and improved CO<sub>2</sub> storage capacity by 1.9%–14.0%. and increased the feasibility and effect of CO<sub>2</sub> storage and production enhancement by injecting CO<sub>2</sub> into the hydraulically fractured coal seam.

It is recognised that although this paper contains a lot of new data, further work needs to be carried out to elucidate the more detailed mechanisms to which the data hint. The presence of coal fines inhibits gas flow by increasing the tortuosity of flow pathways, hence reducing channelling. However, coal fines also introduce a phase with a huge surface area for adsorption relative to its volume, providing additional adsorption capacity that is immediately accessible to CO<sub>2</sub> in the flow pathway.

Depleted coalbed methane reservoirs are prime targets for  $CO_2$  sequestration, offering accessible rock matrix often with high permeabilities and large surface areas for  $CO_2$  adsorption. These potential  $CO_2$  depositories have undergone a complex history of exploitation that often includes water and methane flow as well as hydraulic stimulation. This work has managed to make measurements taking all of these variables into account, including the relative presence of coal fines. As such the data should be of great interest to the commercial operators interested in using such complex entities for  $CO_2$  storage. The measurements made in this work simulate  $CO_2$  injection through propped and unpropped fractures and then into the coal matrix. On this basis alone, the work has great applicability in understanding these complex and inter-related  $CO_2$  emplacement processes.

# **CRediT authorship contribution statement**

Qian Wang: Writing — original draft, Resources, Methodology, Investigation, Funding acquisition. Zhi-Jun Zhang: Writing — review & editing, Writing — original draft, Resources, Methodology. Jian-Long Xiong: Writing — review & editing, Resources. Jian Shen: Writing — review & editing, Resources, Funding acquisition. Paul W.J. Glover: Writing — review & editing. Piroska Lorinczi: Writing — review & editing.

#### **Declaration of competing interest**

The authors declare that they have no known competing financial interests or personal relationships that could have appeared to influence the work reported in this paper.

# Acknowledgments

This research is supported by National Natural Science Foundation of China (52104048, 42272198).

#### References

- Bai, T., Chen, Z., Aminossadati, S., Rufford, T., Li, L., 2017. Experimental investigation on the impact of coal fines generation and migration on coal permeability. J. Petrol. Sci. Eng. 159, 257–266. https://doi.org/10.1016/j.petrol.2017.09.035.
- Busch, A., Gensterblum, Y., Krooss, B.M., Littke, R., 2004. Methane and carbon dioxide adsorption—diffusion experiments on coal: upscaling and modeling. Int. J. Coal Geol. 60 (2–4), 151–168. https://doi.org/10.1016/j.coal.2004.05.002.
- Cheng, Y., Liu, Q., Ren, T., 2021. Gas adsorption—desorption properties of coal. Coal Mechanics 111–150. https://doi.org/10.1007/978-981-16-3895-4\_4.
- Cheng, Y., Pan, Z., 2020. Reservoir properties of Chinese tectonic coal: a review. Fuel 260, 116350. https://doi.org/10.1016/j.fuel.2019.116350.
- Clarkson, C.R., Bustin, R.M., 2010. Coalbed methane: current evaluation methods, future technical challenges. In: SPE Unconventional Resources Conference/Gas Technology Symposium. https://doi.org/10.2118/72274-JPT.
- Danso, D.K., Negash, B.M., Ahmed, T.Y., Yekeen, N., Ganat, T.A.O., 2021. Recent advances in multifunctional proppant technology and increased well output with micro and nano proppants. J. Petrol. Sci. Eng. 196, 108026. https://doi.org/10.1016/j.petrol.2020.108026.
- De Silva, P.N.K., Ranjith, P.G., Choi, S.K., 2012. A study of methodologies for CO<sub>2</sub> storage capacity estimation of coal. Fuel 91 (1), 1–15. https://doi.org/10.1016/j.fuel.2011.07.010.
- Du, X., Cheng, Y., Liu, Z., Yin, H., Wu, T., Huo, L., Shu, C., 2021. CO<sub>2</sub> and CH<sub>4</sub> adsorption on different rank coals: a thermodynamics study of surface potential, Gibbs free energy change and entropy loss. Fuel 283, 118886. https://doi.org/10.1016/j.fuel.2020.118886.
- Fan, C., Elsworth, D., Li, S., Chen, Z., Luo, M., Song, Y., Zhang, H., 2019a. Modelling and optimization of enhanced coalbed methane recovery using CO<sub>2</sub>/N<sub>2</sub> mixtures. Fuel 253, 1114–1129. https://doi.org/10.1016/j.fuel.2019.04.158.
- Fan, C., Elsworth, D., Li, S., Zhou, L., Yang, Z., Song, Y., 2019b. Thermo-hydro-mechanical-chemical couplings controlling CH<sub>4</sub> production and CO<sub>2</sub> sequestration in enhanced coalbed methane recovery. Energy 173, 1054–1077. https://doi.org/ 10.1016/j.energy.2019.02.126.
- Fan, Z., Fan, G., Zhang, D., Zhang, L., Zhang, S., Liang, S., Yu, W., 2021. Optimal injection timing and gas mixture proportion for enhancing coalbed methane recovery. Energy 222, 119880. https://doi.org/10.1016/j.energy.2021.119880.
- Feng, D., Guo, D., Zhang, Y., Sun, S., Zhao, Y., Chang, G., Qin, Y., 2021. Adsorption-enrichment characterization of CO<sub>2</sub> and dynamic retention of free NH<sub>3</sub> in functionalized biochar with H<sub>2</sub>O/NH<sub>3</sub>·H<sub>2</sub>O activation for promotion of new ammonia-based carbon capture. Chem. Eng. J. 409, 128193. https://doi.org/10.1016/j.cej.2020.128193.
- Guo, Z., Hussain, F., Cinar, Y., 2016. Physical and analytical modelling of permeability damage in bituminous coal caused by fines migration during water production.

  J. Nat. Gas Sci. Eng. 35, 331–346. https://doi.org/10.1016/j.jngse.2016.08.031.
- Guo, Z., Vu, P.N.H., Hussain, F., 2018. A laboratory study of the effect of creep and fines migration on coal permeability during single-phase flow. Int. J. Coal Geol. 200, 61–76. https://doi.org/10.1016/j.coal.2018.10.009.
- Han, W., Wang, Y., Li, Y., Ni, X., Wu, X., Yang, J., Zhao, S., 2021. Coal fines migration, deposition, and output simulation during drainage stage in coalbed methane production. Energy & Fuels 35 (6), 4901–4913. https://doi.org/10.1021/acs.energyfuels.0c04418.
- Han, Z., Lyu, S., Lu, A., Chen, L., Chen, Q., Xing, H., 2024. Agglomeration-dispersion effects of coal fines to control the permeability of propping fractures: a visual experimental study. Gas Science and Engineering 131, 205474. https://doi.org/ 10.1016/j.jgsce.2024.205474.
- Hu, Q., Liu, L., Li, Q., Wu, Y., Wang, X., Jiang, Z., Wu, X., 2020. Experimental investigation on crack competitive extension during hydraulic fracturing in coal measures strata. Fuel 265, 117003. https://doi.org/10.1016/j.fuel.2019.117003.
- Huang, F., Kang, Y., You, Z., You, L., Xu, C., 2017. Critical conditions for massive fines detachment induced by single-phase flow in coalbed methane reservoirs: modeling and experiments. Energy & Fuels 31 (7), 6782–6793. https://doi.org/ 10.1021/acs.energyfuels.7b00623.
- Huang, F., Dong, C., Shang, X., You, Z., 2021. Effects of proppant wettability and size on transport and retention of coal fines in saturated proppant packs: experimental and theoretical studies. Energy & Fuels 35 (15), 11976—11991. https:// doi.org/10.1021/acs.energyfuels.1c01418.
- Huang, F., Wang, F., Chen, F., Sang, S., Liu, S., You, Z., 2024. Transport and retention of coal fines in proppant packs during gas-water two-phase flow: insights from

- interface, pore, to laboratory scales. Energy & Fuels 38 (14), 12672–12683. https://doi.org/10.1021/acs.energyfuels.4c02255.
- Jin, F., Chen, S., Wei, B., Wang, D., Yang, W., Wang, Y., Lu, J., 2021. Visualization of CO<sub>2</sub> foam generation, propagation and sweep in a complex 2D heterogeneous fracture network. Fuel 302, 121000. https://doi.org/10.1016/j.fuel.2021.121000.
- Li, H., Wu, M., Liu, Z., Wang, F., Yang, N., Lou, R., Yu, Y., 2022. Permeation-diffusion characteristics and air-leakage blocking mechanism for the fire-extinguishing inorganic gel flows in loose broken coal particles. Fuel 328, 125245. https:// doi.org/10.1016/j.fuel.2022.125245.
- Li, S., Tang, D., Pan, Z., Xu, H., Tao, S., Liu, Y., Ren, P., 2018. Geological conditions of deep coalbed methane in the eastern margin of the Ordos Basin, China: implications for coalbed methane development. J. Nat. Gas Sci. Eng. 53, 394–402. https://doi.org/10.1016/j.jngse.2018.03.016.
- Li, S., Qin, Y., Tang, D., Shen, J., Wang, J., Chen, S., 2023. A comprehensive review of deep coalbed methane and recent developments in China. Int. J. Coal Geol., 104369 https://doi.org/10.1016/j.coal.2023.104369.
- Lin, H., Ji, P., Kong, X., Li, S., Long, H., Xiao, T., Li, B., 2023. Experimental study on the influence of gas pressure on CH<sub>4</sub> adsorption-desorption-seepage and deformation characteristics of coal in the whole process under triaxial stress. Fuel 333, 126513. https://doi.org/10.1016/j.fuel.2022.126513.
- Lin, X., Liu, Z., Zhu, W., Zhao, T., Liu, S., Sun, C., Bai, G., Zhang, Y., 2024. Investigation on coal permeability evolution considering the internal differential strain and its effects on CO<sub>2</sub> sequestration capacity in deep coal seams. Energy 304, 132026. https://doi.org/10.1016/j.energy.2024.132026.
- Liu, S., Fang, H., Sang, S., Ashutosh, T., Wu, J., Zhang, S., Zhang, B., 2020. CO<sub>2</sub> injectability and CH<sub>4</sub> recovery of the engineering test in Qinshui Basin, China based on numerical simulation. Int. J. Greenh. Gas Control 95, 102980. https://doi.org/10.1016/j.ijggc.2020.102980.
- Lv, Q., Zhou, T., Zhang, X., Zuo, B., Dong, Z., Zhang, J., 2020. Enhanced oil recovery using aqueous CO<sub>2</sub> foam stabilized by particulate matter from coal combustion. Energy & Fuels 34 (3), 2880–2892. https://doi.org/10.1021/acs.energyfuels.9b04066.
- Ma, T., Liu, J., Fu, J., Wu, B., 2022. Drilling and completion technologies of coalbed methane exploitation: an overview. International Journal of Coal Science & Technology 9 (1), 68. https://doi.org/10.1007/s40789-022-00540-x.
- Mazumder, S., Wolf, K.H., 2008. Differential swelling and permeability change of coal in response to CO<sub>2</sub> injection for ECBM. In: SPE Asia Pacific Oil and Gas Conference and Exhibition. https://doi.org/10.1016/j.coal.2007.11.001.
- Qin, Y., Moore, T.A., Shen, J., Yang, Z., Shen, Y., Wang, G., 2020. Resources and geology of coalbed methane in China: a review. Coal Geology of China, pp. 247–282.
- Rezk, M.G., Foroozesh, J., 2022. Uncertainty effect of CO<sub>2</sub> molecular diffusion on oil recovery and gas storage in underground formations. Fuel 324, 124770. https:// doi.org/10.1016/j.fuel.2022.124770.
- Rezk, M.G., Ibrahim, A.F., Adebayo, A.R., 2023. Uncertainty quantification for CO<sub>2</sub> storage during intermittent CO<sub>2</sub>-EOR in oil reservoirs. Int. J. Coal Geol. 266, 104177. https://doi.org/10.1016/j.coal.2022.104177.
- Shi, Q., Qin, Y., Zhou, B., Zhang, M., Wu, M., Wang, L., 2018. An experimental study of the agglomeration of coal fines in suspensions: inspiration for controlling fines in coal reservoirs. Fuel 211, 110–120. https://doi.org/10.1016/j.fuel.2017.09.044.
- Song, Z., Hou, J., Liu, X., Wei, Q., Hao, H., Zhang, L., 2018. Conformance control for CO<sub>2</sub>-EOR in naturally fractured low permeability oil reservoirs. J. Petrol. Sci. Eng. 166, 225–234. https://doi.org/10.1016/j.petrol.2018.03.030.
- Sun, W., Lin, H., Li, S., Kong, X., Long, H., Yan, M., Tian, J., 2021. Experimental research on adsorption kinetic characteristics of CH<sub>4</sub>, CO<sub>2</sub>, and N<sub>2</sub> in coal from Junggar Basin, China, at different temperatures. Natural Resources Research 30, 2255–2271. https://doi.org/10.1007/s11053-021-09812-w.
- Wang, D., Wang, Z., Cai, X., 2023. Experimental study on coal fines migration and effects on conductivity of hydraulic fracture during entire coalbed methane production period. Geoenergy Science and Engineering 223, 211555. https://

- doi.org/10.1016/j.geoen.2023.211555.
- Wang, G., Jiang, C., Shen, J., Han, D., Qin, X., 2019. Deformation and water transport behaviors study of heterogenous coal using CT-based 3D simulation. Int. J. Coal Geol. 211, 103204. https://doi.org/10.1016/j.coal.2019.05.011.
- Wang, Q., Shen, J., Lorinczi, P., Glover, P.W., Yang, S., Chen, H., 2021. Oil production performance and reservoir damage distribution of miscible CO<sub>2</sub> soakingalternating-gas (CO<sub>2</sub>-SAG) flooding in low permeability heterogeneous sandstone reservoirs. J. Petrol. Sci. Eng. 204, 108741. https://doi.org/10.1016/ j.petrol.2021.108741.
- Wang, Q., Zhu, B., Shen, J., Glover, P.W., Lorinczi, P., Han, H., 2022a. Quantifying controls on threshold pressure during CO<sub>2</sub> injection in tight gas reservoir rocks. Energy & Fuels 36 (12), 6292–6304. https://doi.org/10.1021/acs.energyfuels.2c01307.
- Wang, Q., Shen, J., Glover, P.W., Lorinczi, P., Zhao, W., 2022b. Oil production enhancement, asphaltene precipitation and permeability damage during CO<sub>2</sub>-SAG flooding of multi-layer sandstone reservoirs. J. Petrol. Sci. Eng. 212, 110241. https://doi.org/10.1016/j.petrol.2022.110241.
- Wang, R., Wang, Q., Niu, Q., Pan, J., Wang, H., Wang, Z., 2020. CO<sub>2</sub> adsorption and swelling of coal under constrained conditions and their stage-change relationship. J. Nat. Gas Sci. Eng. 76, 103205. https://doi.org/10.1016/j.jingse.2020.103205.
- Wang, Z., Liu, S., Qin, Y., 2021. Coal wettability in coalbed methane production: a critical review. Fuel 303, 121277. https://doi.org/10.1016/j.fuel.2021.121277.
- Wei, Y., Li, C., Cao, D., Wang, A., Zhang, A., Yao, Z., 2019. The effects of particle size and inorganic mineral content on fines migration in fracturing proppant during coalbed methane production. J. Petrol. Sci. Eng. 182, 106355. https://doi.org/ 10.1016/j.petrol.2019.106355.
- Xiong, J., Zhang, Z., Wang, Q., Shen, J., Glover, P.W., Lorinczi, P., Zhang, J., Zheng, S., 2024. Influence of coal stress sensitivity on the desorption production characteristics and residual CH<sub>4</sub> distribution of thin multilayered coal seams. Energy & Fuels 38 (23), 22820–22832. https://doi.org/10.1021/acs.energyfuels.4c03872.
- Yang, Q., Xue, J., Li, W., Hu, B., Ma, Q., Zhan, K., Du, X., Chen, Z., 2022. Reconstructions of supercritical CO<sub>2</sub> adsorption isotherms and absolute adsorption estimation in nanoporous coals considering volumetric effects and varying adsorbed phase densities. Chem. Eng. J. 433, 133492. https://doi.org/10.1016/j.cej.2021.133492.
- Yang, Z., Li, W., Pei, Y., Qiao, W., Wu, Y., 2018. Classification of the type of ecogeological environment of a coal mine district: a case study of an ecologically fragile region in Western China. J. Clean. Prod. 174, 1513—1526. https://doi.org/ 10.1016/j.jclepro.2017.11.049.
- Zhang, C.P., Liu, S., Ma, Z.Y., Ranjith, P.G., 2021. Combined micro-proppant and supercritical carbon dioxide (SC-CO<sub>2</sub>) fracturing in shale gas reservoirs: a review. Fuel 305, 121431. https://doi.org/10.1016/j.fuel.2021.121431.
- Zhang, H., Shen, J., Wang, G., Li, K., Fang, X., 2023. Experimental study on the effect of high-temperature nitrogen immersion on the nanoscale pore structure of different lithotypes of coal. Energy 284, 128596. https://doi.org/10.1016/j.energy.2023.128596.
- Zhang, X., Ranjith, P.G., 2019. Experimental investigation of effects of CO<sub>2</sub> injection on enhanced methane recovery in coal seam reservoirs. J. CO<sub>2</sub> Util. 33, 394–404. https://doi.org/10.1016/j.jcou.2019.06.019.
- Zhu, G., Zhao, Y., Zhang, T., Khalid, M.S.U., Liu, M., Zhang, S., Zhang, Z., 2023. Microscale reconstruction and CFD-DEM simulation of proppant-laden flow in hydraulic fractures. Fuel 352, 129151. https://doi.org/10.1016/j.fuel.2023.129151.
- Zhu, S., Peng, X., Du, Z., Wang, C., Deng, P., Mo, F., Lei, Y., Wang, M., 2017. Modeling of coal fine migration during CBM production in high-rank coal. Transport Porous Media 118, 65–83. https://doi.org/10.1007/s11242-017-0847-7.
- Zou, Y., Zhang, S., Zhan, J., 2014. Experimental method to simulate coal fines migration and coal fines aggregation prevention in the hydraulic fracture. Transport Porous Media 101, 17—34. https://doi.org/10.1007/s11242-013-0228-9.